Ninth International Conference on CFD in the Minerals and Process Industries
CSIRO, Melbourne, Australia
10-12 December 2012

SIMULATION OF FLOW IN A HELICAL DEVICE USED FOR IRRADIATING BIOLOGICAL FLUIDS

Mahesh PRAKASH[1*], Todd NIKOLOF[2], Paul W. CLEARY[1] and Joseph BERTOLINI[2]

[1] CSIRO Mathematics, Informatics and Statistics, Clayton, Victoria 3169, AUSTRALIA

[2] CSL Biotherapies, 189-209 Camp Road, Broadmeadows, Victoria 3047, AUSTRALIA
*Corresponding author, E-mail address: Mahesh.Prakash@csiro.au

ABSTRACT

Plasma based therapeutic products must undergo viral inactivation steps in order to minimize the risk of infection. Non-enveloped viruses such as hepatitis A and parvovirus are more recently being inactivated by using Ultra Violet light C (UV-C) irradiation techniques. A commonly used form of UV-C irradiation involves passing the protein solution through a helical tube that wraps around an irradiation source. The helical nature of the tube allows the formation of two counter-rotating Dean vortices along the cross-section of the helix. These ensure controlled mixing of the fluid leading to uniform exposure to UV-C irradiation. A detailed assessment of Dean vortices in a helical tube is performed in this paper using the Smoothed Particle Hydrodynamics (SPH) method. SPH being a Lagrangian Computational Fluid Dynamic (CFD) method is particularly well suited for evaluating history dependent properties such as residence time distribution of the fluid as it transits such a device. The simulations provided a basis for setting flow rate limits for the laboratory scale apparatus. Experimentally recorded UV inactivation rates using chemical actinometry led to a very good match with simulations. Results indicate that for the laboratory scale equipment the Dean vortex structure is absent for flow rates above 10 l/hr leading to reduced efficiency of UV-C irradiation. It is shown that the operating range of the laboratory scale device can be extended to at least until 25 l/hr by altering the cross-sectional shape of the tube. Simulations were also performed for the process scale device to investigate the effect of scaling up the size of the device on the Dean vortex pattern. Dean vortices were present in this case for the entire flow rate range from 5 to 40 l/hr.

INTRODUCTION

The manufacture process for blood plasma derived therapeutic products must always include dedicated viral inactivation steps to minimize the risk of infection as stipulated by WHO in (2004). Typical viral removal and inactivation methods employed include dry heat treatment; Kim et al. (2008), pasteurisation; Adcock et al. (1998), low-pH incubation; Johnston et al. (2003), nanofiltration and treatment with solvent/detergent; Johnston et al. (2000) and caprylate as a stabiliser; Johnston et al. (2003). These methods are very effective for enveloped viruses such as hepatitis B & C and human immunodeficiency virus (HIV) but generally less effective against small, non-enveloped viruses, such as hepatitis A virus (HAV) or parvovirus B19 as shown by Kim et al. (2008) and Wang et al. (2004). A more effective means of removal or inactivation of the later class of viruses is required.

There has been interest in the use of UltraViolet light C (UV-C) irradiation as a means of inactivation for both enveloped and non-enveloped viruses (Hart et al., 1993 and Wang et al., 2004). An early UV-C device involved exposing biological fluids in the form of thin flowing films to a controlled UV irradiation source as described in Wolf et al. (1947) and used more recently by Schmidt et al. (2005). However, this approach has limited volume throughput, and requires prolonged exposure of material to UV-C, leading to protein damage through the generation of free radicals and heat as shown by Streeter and Gordon (1967). Alternative approaches for activation have now been developed which have made UV-C irradiation a viable viral inactivation procedure. These include the Iatros UV virus inactivation system, which involves passing protein solutions through a transparent tube around which UV-C lamps are arranged as demonstrated by Altic et al. (2007). The utilization of a static mixer ensures efficient and uniform mixing of the protein solution. With the UVivatec lab system (Bayer Technology Services), the protein solution flows through a spiral tube around an irradiation source. This was used by Wang et al. (2004) in their inactivation trials. Two counter-rotating vortices across the cross-section of the spiral tube are formed for a range of flow rates. These produce controlled mixing and a relatively uniform exposure to UV-C. These are referred to as Dean vortices (Moll et al.; 2002).

A detailed investigation of Dean vortices in the UVivatec system has been performed so far. At the laboratory scale, this analysis is needed to provide a basis for setting flow rate limits for experimental investigation of viral inactivation. Simulations at the process scale are also performed to investigate the effect of scaling up the device on the Dean vortex pattern.

Smoothed Particle Hydrodynamics (SPH) is a Lagrangian fluid simulation method that has been used to model various fluid flows in the bio-processing industry such as analysing stress levels and flow characteristics of human albumin through a lobe pump by Gomme et al. (2006), bioreactor mixing by Fang et al. (2010) and pharmaceutical cleaning by Gafford et al. (2010). SPH has been used here to predict the flow of liquids in the UVivatec irradiation chamber for various flow rates at laboratory and process scales. The effect of flow rate related changes in fluid dynamics on the irradiation dose (fluence) was also investigated by chemical actinometry studies. Experimentally, the presence of Dean vortices will

lead to a linear increase in the fluence rate with flow rate. On the other hand a breakdown of the Dean vortex structure will result in a plateauing of the fluence rate. This was used to provide empirical evidence for the effect of flow rate and Dean vortex formation on delivered UV-C dose and for comparison against the simulated lab scale results.

MODEL GEOMETRY

Computer aided design (CAD) models consisting of four turns of the coil for the laboratory and process scale instruments were created based on line drawings supplied by Bayer Technologies (Leverkusen, Germany). The lab and process scale geometries are identical except for the scaling. The CAD model for the spiral tube is shown in Figure 1.

The cross-sectional geometries used in the simulations are shown in Figure 2. The cross-section shown in frame a of Figure 2 is used for the UVivatec lab and process scale systems. The semi-circular cross-section shown in frame b of Figure 2 is a proposed alternative for the lab-scale system. Flow is established in the coil by using an inflow boundary condition at the lower end of the coil. The fluid enters the coil with a close to parabolic profile. The Reynolds number (Re), defines the flow regime experienced in the irradiation chamber. This is defined as:

$$\mathrm{Re} = \frac{DU\rho}{\mu} \qquad (1)$$

where D is the internal diameter of the helical coil, U is the mean fluid velocity in the coil calculated using the flow rate, ρ is the fluid viscosity assumed here to be the same as water (1000 kg/m^3) and μ is the fluid viscosity assumed to be the same as water (10^{-3} Pa s). This is realistic for plasma products. The lab scale has an internal diameter of 4 mm whereas the process scale has an internal diameter of 7 mm.

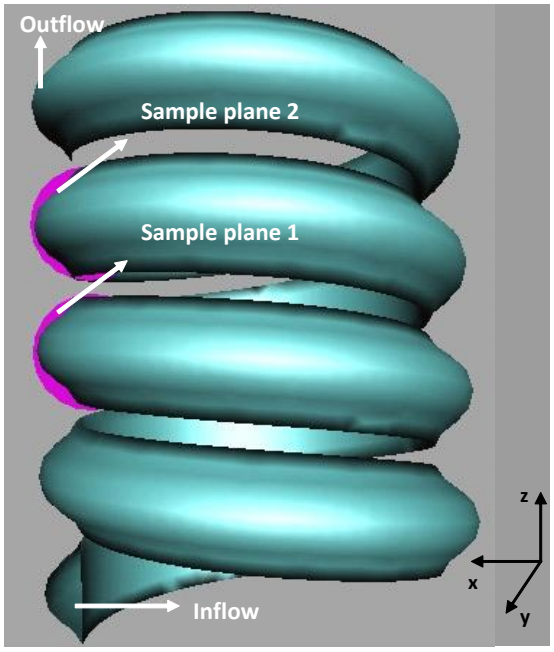

Figure 1: 3D CAD model of the UV helical device. Four turns of the coil are illustrated. Inflow, outflow and two sample planes are shown.

Based on this definition Re is between 500 and 5000 for the lab scale device for flow rates of 2 to 20 l/hr. For the process scale device, Re is between 540 and 4320 for flow rates of 5 to 40 l/hr. This suggests that a range of 2 to 20 l/hr in the lab scale is comparable to a range of 5 to 40 l/hr for the process scale from a Re similarity perspective. The process scale simulations are therefore performed for a 5 to 40 l/hr range. The volumetric flow rate is specified at the inflow. Fluid passes through the four turns of the coil and then exits the coil through the outflow boundary condition at the upper end of the coil, as shown in Figure 1. Sample plane 1 is where the averaged velocity and shear stress data is collected. Fluid residence time for one complete turn of the coil is measured between sample plane 1 and 2.

Fluid flow through the irradiation chamber consists of three velocity components. One component is the azimuthal velocity which follows the angle of the spiralling irradiation chamber in the primary direction of flow. The secondary flow is made up of the radial and axial velocity components.

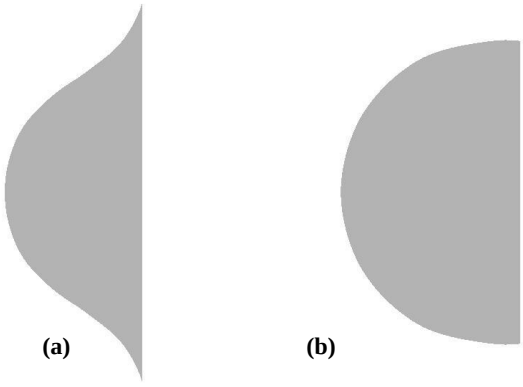

Figure 2: Tube cross-sections for (a) UVivatec lab and process scale systems and (b) alternative lab scale version.

SPH METHOD AND MODEL SETUP

Computational fluid dynamic simulations of the UVivatec irradiation chamber were performed using the SPH method. The numerical method is described in detail in Monaghan (1994) and Cleary et al. (1999). SPH is a mesh free method for modelling fluid flows and heat transfer. The fluid is approximated by particles that move with the flow rather than by fixed grids or meshes. It is based on Lagrangian concepts and is particularly well suited for evaluating history dependent properties such as the residence time distribution of the fluid as it passes through the coils of the helical device. The shear stress experienced by the fluid as it passes through the helical coil is calculated using the technique previously described in Gomme et al. (2006).

An SPH particle resolution of 0.15 mm is used here for all simulations following a study to ensure results are acceptably independent of the SPH resolution chosen. The number of fluid particles to fill four winds of the helical coil for the lab and process scale devices is approximately 350,000 and 1 million respectively.

The Re varies between 500 and 5000 for the flow rates used here. The flow therefore begins at the laminar regime

but could possibly be transitional to a turbulent regime for Re = 5000.

ESTABLISHMENT OF STEADY FLOW

The steady state behaviour of the flow was established by ensuring that the total kinetic energy of the fluid in the system had reached a steady value. The kinetic energy plot for the highest flow rate of 20 l/hr for the lab scale device is shown in Figure 3a. It reached an almost constant value after around 0.3 s of simulation. By this stage the fluid velocity measured at the sample plane had also reached a steady state as shown in Figure 3b. The flow rate specified at the inflow and measured at the sample plane at steady state matched to within 0.2%. The density variation was less than 0.4% for the flow rates investigated. Together, they ensure that SPH conditions required for the fluid to be considered homogenous and incompressible are met.

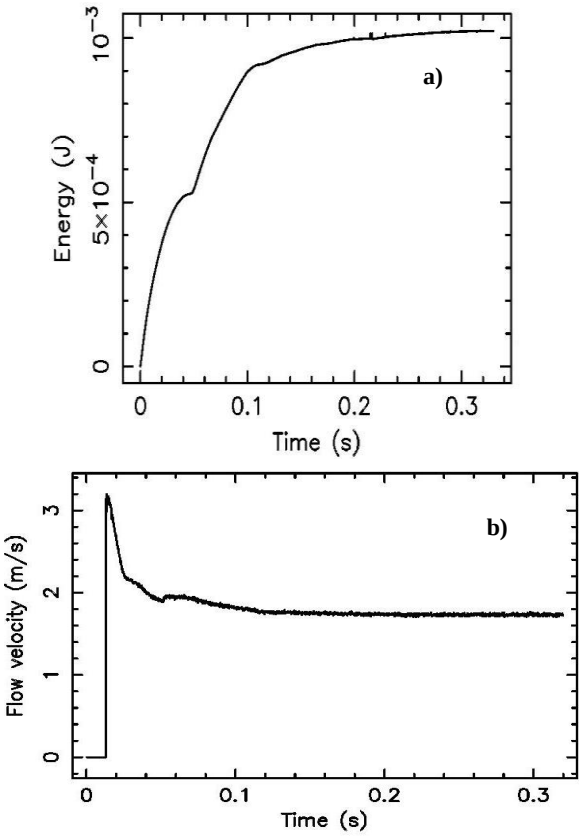

Figure 3: Time variation for a 20 l/hr flow rate of (a) fluid kinetic energy, and (b) average fluid velocity measured at the two sample planes. The flow becomes steady at 0.3 s.

ANALYSIS OF FLOW AND RESIDENCE TIME

A cartesian grid is used to collect velocity and shear stress data over the flow domain. Data is presented for a slice corresponding to sample plane 1 in Figure 1. The grid has square cells with a side length of 0.2 mm. For each flow rate data is collected on this grid once steady state behaviour is established as described in the previous section. The data is time averaged for a sufficient duration until the velocity and shear stress plots show an invariant pattern and the magnitudes converge to a constant value.

Averaged data collected at sample plane 1 consists of the radial velocity in the *x* direction, axial velocity in the *z* direction, azimuthal velocity in the *y* direction (as shown in Figure 1) and the shear stress. The velocity vector plot consists of the radial and axial components across the sample plane.

EXPERIMENTS

All UV-C experiments were performed in a UVivatec lab system. A poly(tetrafluorethylene) tube, which spirals around a quartz tube containing the UV-C source (wavelength of 254 nm), forms the irradiation chamber of the device. The irradiation surface area is 0.0246 m^2 and the volume of the irradiation chamber is 24 ml.

Determination of UV fluency

Iodide-Iodate chemical actinometry solutions were prepared as described in Rahn (2004). The iodide-iodate actinometry solution consisted of 0.6M potassium iodide, 0.1M potassium iodate and 0.01M sodium tetraborate decahydrate with a pH of 9.2.

A 40 ml aliquot of the actinometric solution was irradiated in the UVivatec lab system at various flow rates. The first 10 ml of each sample was discarded, and the following 10 ml was collected for analysis of UV-C exposure extent. Non-irradiated potassium iodide was used to zero the Cary 50 spectrophotometer at 352 nm. All irradiated samples were diluted with non-irradiated actinometric solution, and the absorbances of diluted samples were measured at 352 nm. Chemical actinometry experiments for each flow tested were performed in triplicate, and fluence was calculated as described in Rahn (2004).

PREDICTED FLOW STRUCTURE

The helical nature of the coil with an inclination in the positive *z* direction (as shown in Figure 1) gives rise to an average bulk velocity. It is important to subtract the average bulk velocity (which constitutes the primary flow) from the axial velocity in order to identify the weaker secondary flow. The secondary flow promotes mixing in the helix. The average bulk velocity was obtained by spatially averaging the axial velocity of all fluid elements in one turn of the helix after a steady state was reached. The calculated bulk velocity matched to within 3% of the theoretical value for all three flow rates.

Figure 4 shows the vector plot of velocity at sample plane 1 comprising the radial and secondary axial velocity components. The top row is for the lab scale (case A), middle row is for the lab scale with an alternative cross-section (case B) and the bottom row is for the process scale.

For the lab scale case A, at 2 l/hr the vector plot clearly shows that there are two vortex structures. The first vortex occurs at the top right corner of the helix cross-section with the fluid moving clockwise. The second vortex occurs nearer the bottom left corner of the cross-section with a counter clockwise fluid motion. This secondary flow pattern has similar features to Dean vortices of two counter-rotating vortices found in curved channels and helical tubes as reported in Moll et al. (2002). At 5 l/hr the Dean vortex pattern becomes slightly weaker. As Re increases with an increase in flow rate to 10 l/hr this vortex pattern almost completely disappears with only a very weak vortex in the lower left corner of the cross-section.

For case B, there are two vortex structures in the secondary flow for all three flow rates. The vortex on the top right corner moves away from the wall with an increase in the flow rate from 2 to 10 l/hr. It has a more or less constant shape and position as the flow rate increases from 10 to 20 l/hr. The position of the bottom left vortex does not change significantly with flow rate for the range simulated. The Dean vortex structure persists for the entire flow rate range of 2 to 25 l/hr investigated in the simulations

For the process scale, there are two vortex structures in the secondary flow for all three flow rates. The position of these vortices does not change significantly for the flow rate range simulated.

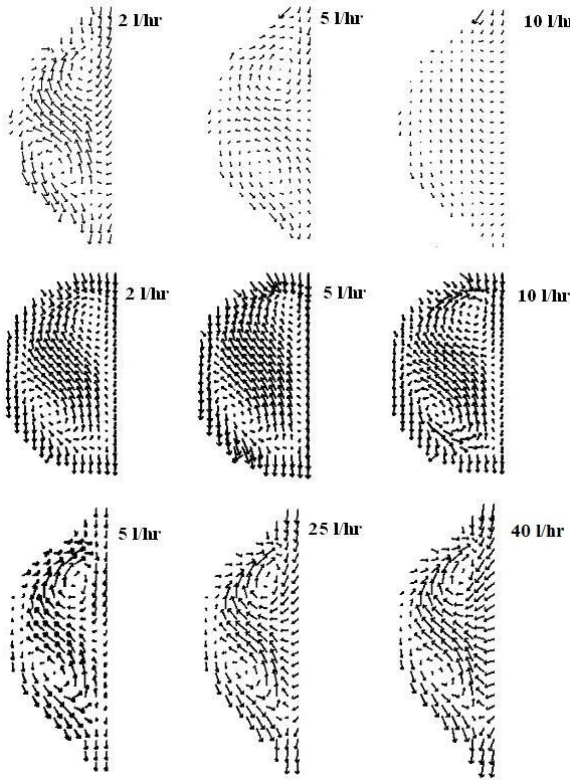

Figure 4: Velocity vectors at sample plane 1 (as shown in Figure 1) of the helical tube for various flow rates. Top row is for the lab scale, case A. Middle row is for the lab scale with an alternative cross-section, case B. Bottom row is for the process scale.

In summary, all velocity plots with the exception of case A, at the highest flow rate of 10 l/hr shows the presence of two vortex structures in the secondary flow, which have characteristic Dean vortex structure.

The lab system has a manufacturer prescribed flow rate range of 2 to 20 l/hr. The two counter rotating vortex structures are present only at 2 and 5 l/hr. Since these are principally responsible for generating mixing then this suggests that reliable controlled mixing for the lab system can only be expected until a flow rate of 10 l/hr. This is lower than its designed maximum of 20 l/hr.

RESIDENCE TIME DISTRIBUTION

Figure 5 shows the residence time distribution of the fluid as it passes through one whole turn of the helical coil for the three cases evaluated. These measurements were made between sample plane 1 and 2 as shown in Figure 1.

For the lab scale case A and process scale devices there is only a single dominant peak in the residence time distribution for the flow rate range analysed. For case A the peak occurs at 0.35, 0.12 and 0.06 s at flow rates of 2, 5 and 10 l/hr. At 2 l/hr only 24% of the fluid is at the peak residence time whereas at 10 l/hr this increases to 62% of the fluid. For the process scale the peak occurs at 0.82, 0.16 and 0.11 s at flow rates of 5, 25 and 40 l/hr. At 5 l/hr only 13% of the fluid is at the peak residence time whereas this increases significantly to 68% of the fluid at 40 l/hr. This suggests that for both these cases the residence time distribution becomes sharper at higher flow rates leading to a significant amount of fluid flowing as one bulk.

For the lab scale case B, however, there is a secondary smaller peak which has a longer residence time compared to the primary peak. The secondary peak is between 12 and 22% of the total fluid volume for the flow rate range of 2 to 10 l/hr. The presence of the secondary peak is related to the existence of isolated region(s) in the modified lab scale system. Fluid in this region is not able to interact with the Dean vortices resulting in reduced mixing. Further modifications to the lab scale system is therefore required in order to eliminate these isolated region(s) while maintaining the Dean vortex structure intact for the flow rate range considered.

SHEAR STRESS

Fluids treated in the helical device are typically plasma products which are prone to suffer damage in prolonged high shear stress environments. Although only the presence of a high shear region need not lead to damage such zones can be a contributing factor. Therefore in addition to achieving uniform irradiation another important consideration is to investigate shear stress levels at various flow rates.

Figure 6 shows the shear stress at sample plane 1 for the lab system, case A (top row), lab system, case B (middle row) and the process system (bottom row). The shear stresses are lower close to the centre of the cross-section and increase with proximity to the walls. Comparison of maximum shear stress levels for the two lab scale geometries shows that case B has values at least 10 times smaller than for case A for all flow rates simulated. Interestingly shear stress levels experienced in the process scale system are lower than the lab scale case A. This is because although the velocities in the lab scale system are lower, the smaller diameter of the lab scale, leads to larger gradients in velocities. This leads to higher shear especially closer to the walls of the helix.

CHEMICAL ACTINOMETRY

Results of actinometric experiments performed using the lab system is shown in Figure 7 where the fluence rate is plotted against the volumetric flow rate through the coil. The UV dose received by the solution measured against a unit of time is referred to as the fluence rate. This steadily increases from a flow rate of 2 to 10 l/hr.

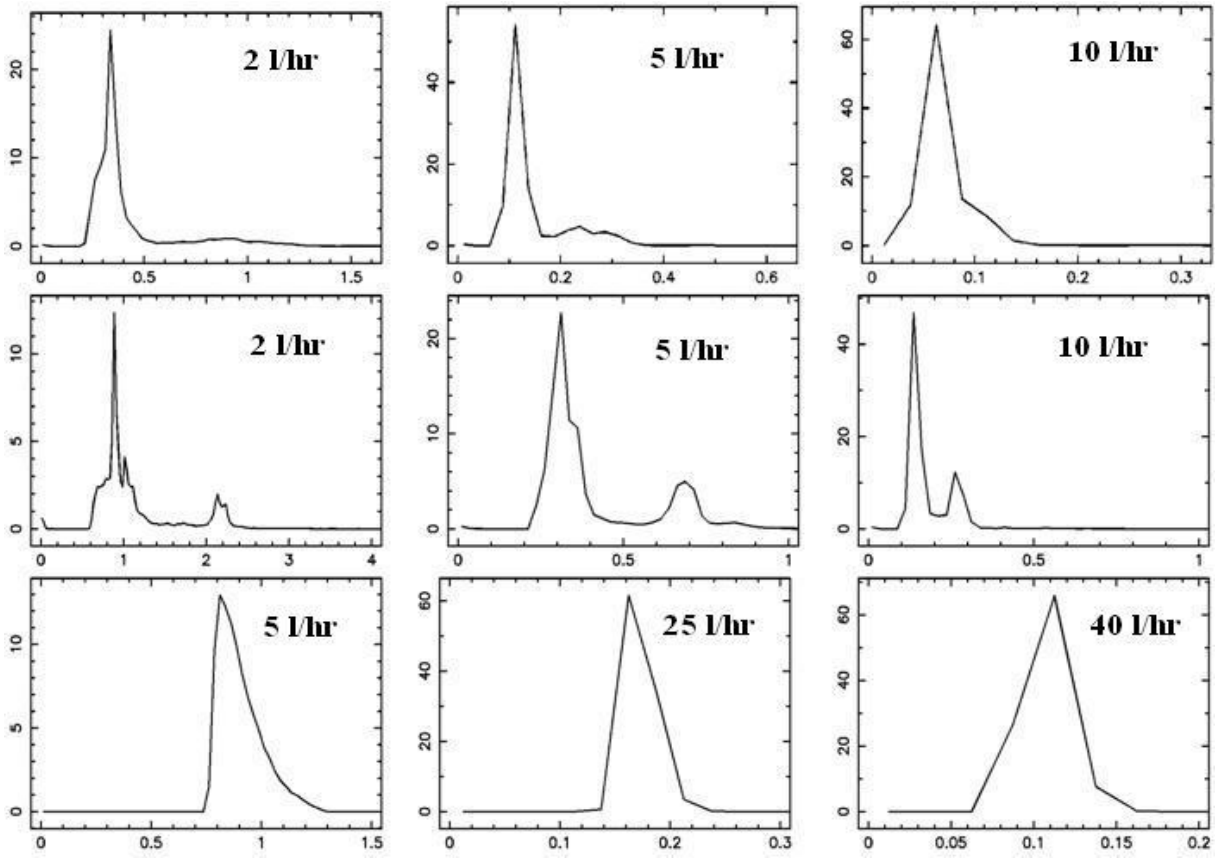

Figure 5: Residence time distribution of the fluid measured between sample planes 1 and 2 (see Figure 1). Top row is for the lab scale cross-section, case A, the middle row is for lab scale cross-section, case B and the bottom row is for process scale.

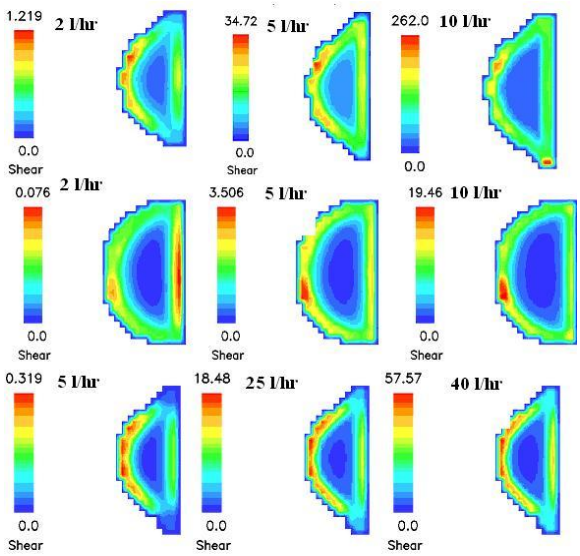

Figure 6: Shear stress for the three geometries modelled. The top row is cross-section A at lab scale. The middle row is lab scale cross-section B. The bottom row is the process scale system. Shear stress is in Pa.

Beyond 10 l/hr, the fluence rate plateaus out. This is consistent with the simulations, which suggests that between 2 to 10 l/hr, as the Dean vortices increases in strength, the efficiency of mixing is increased. The flattening of the fluence rate at around 10 l/hr can be attributed to the dissipation of the Dean vortex structure by a flow rate of 10 l/hr in the simulation as seen in Figure 4, case A.

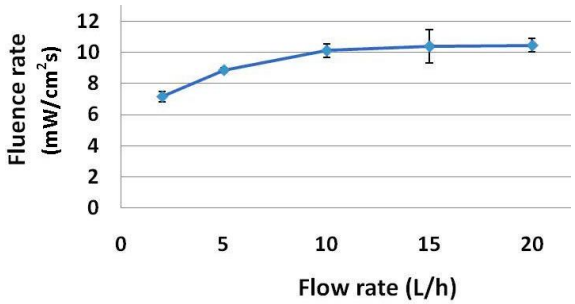

Figure 7: Change in Fluence rate with flow rate for Lab scale system with original cross-section.

CONCLUSIONS

SPH simulations of flow in the helical device used for irradiating protein solutions shows that for the flow rates considered there is a primary flow orthogonal to the cross-section of the helix moving in the azimuthal direction. The helical nature of the coil with an inclination in the axial direction gives rise to an average bulk velocity in this direction. There is a secondary flow in the helix consisting of two circulating vortices across the cross-section of the helix. This has the typical characteristics of Dean vortices encountered in curved channels and helical coils.

For the lab scale UVivatec system the Dean vortex structure breaks down at 10 l/hr. Since Dean vortices are responsible for generating mixing it can be concluded that reliable controlled mixing for the lab system can only be expected until a flow rate of 10 l/hr. This is lower than its

designed maximum of 20 l/hr. For the alternative cross-section lab system the Dean vortex structure persists for the entire flow rate range of 2 to 25 l/hr investigated. This suggests that a moderate modification to the lab scale system can potentially significantly improve its performance over a larger range of flow rates.

For the process scale system the Dean vortex structure persists for flow rates from 5 to 40 l/hr. From a Reynolds number similarity perspective the lab and process scale systems were investigated for a similar range. This shows that the process scale performs better than the UVivatec lab scale over the range of flow rates investigated.

Analysis of residence time distribution for the UVivatec lab and process scales shows that there is only one dominant peak. The distribution becomes sharper at higher flow rates with more than 60% of the fluid at peak residence time at the highest flow rate. For the alternative lab scale cross-section however there is a secondary smaller peak which has a longer residence time compared to the primary peak. The presence of the secondary peak is related to the existence of isolated region(s) where fluid is not able to interact with the Dean vortices resulting in reduced mixing. Further modification to the lab scale system is therefore required in order to eliminate these isolated region(s) while still maintaining the Dean vortex structure.

Comparison of maximum shear stress levels for the two lab scale geometries shows that the alternative cross-section has values at least ten times smaller than for the UVivatec lab system. This provides further encouragement to potentially consider modification of the existing design. Interestingly shear stress levels experienced in the UVivatec process scale system are lower than for the lab scale.

Finally chemical actinometry studies show that the fluence rate steadily increases from a flow rate of 2 to 10 l/hr. Beyond 10 l/hr, the fluence rate plateaus out. This is consistent with the simulations which suggest that by 10 l/hr the Dean vortex structure has started dissipating resulting in poor mixing and therefore reduced efficiency of UV irradiation.

REFERENCES

ADCOCK, W.L., MACGREGOR, A., DAVIES, J.R., HATTARKI, M., ANDERSON, D.A. and GOSS, N.H. (1998) Chromatographic removal and heat inactivation of hepatitis A virus during manufacture of human albumin. *Biotechnol. Appl. Biochem.* **1**, 85-94.

ALTIC, L.C., ROWE, M.T. and GRANT, I.R. (2007) UV Light Inactivation of *Mycobacterium avium* subsp. *paratuberculosis* in Milk as Assessed by *FASTPlaque*TB Phage Assay and Culture http://www.ncbi.nlm.nih.gov/pmc/articles/PMC Appl. Environ. *Microbiol.* **73**, 3728–3733.

CLEARY, P.W. and MONAGHAN, J.J. (1999) Conduction modelling using smoothed particle hydrodynamics. *J. Computat. Phys*. **148**, 227–264.

FANG, Z. (2010) Applying Computational Fluid Dynamics Technology in Bioprocesses-part 1. *BioPharm. Int.* **23**, 42-46

GAFFORD, J., ROBERTS, J. and SULLIVAN, J. (2010) Computational fluid dynamics as a tool for designing quality into the pharmaceutical cleanroom. *Pharmaceut. eng.* **30**, 54-60.

GOMME, P.T., PRAKASH, M., HUNT, B., STOKES, N., CLEARY, P., TATFORD, O.C. and BERTOLINI, J. (2006) Effect of lobe pumping on human albumin: development of a lobe pump simulator using smoothed particle hydrodynamics. *Biotechnol. Appl. Biochem*. **43**, 113-120.

HART, H., REID, K. and HART, W. (1993) Inactivation of viruses during ultraviolet light treatment of human intravenous immunoglobulin and albumin. *Vox Sang*. **64**, 82-88.

JOHNSTON, A., MACGREGOR, A., BOROVEC, S., HATTARKI, M., STUCKLY, K., ANDERSON, D., GOSS, N.H., OATES, A. and UREN, E. (2000) Inactivation and clearance of viruses during the manufacture of high purity factor IX. *Biologicals*. **28**, 129-36.

JOHNSTON, A., UREN E., JOHNSTONE, D. and WU, J. (2003) Low pH, caprylate incubation as a second viral inactivation step in the manufacture of albumin. Parametric and validation studies. *Biologicals*. **31**, 213-221.

KIM, I.S., CHOI, Y.W., KANG, Y., SUNG, H.M. and SHIN, J.S. (2008) Dry-heat treatment process for enhancing viral safety of an antihemophilic factor VIII concentrate prepared from human plasma. *J. Microbiol. Biotechnol*. **18**, 997-1003.

MOLL, R., MOULIN, P.H., VEYRET, D. and CHARBIT, F. (2002) Numerical simulation of Dean vortices: fluid trajectories. *J. of Memr. Sci.* **197**, 157-172.

MONAGHAN, J.J. (1994) Simulating free surface flows using Smoothed Particle Hydrodynamics. *J. Comp. Phys.* **110**, 399-406.

RAHN, R.O. (2004) Spatial distribution of upper-room germicidal UV irradiation as measured with tubular actinometry as compared with spherical actinometry. *Photochem. Photobiol*. **80**, 346-350.

SCHMIDT, S., MORA, J., DOLAN, S. and KAULING, J. (2005). An integrated concept for robust and efficient virus clearance and contamination removal in biotech process. *BioProcess Int.* **3**, 26-31.

STREETER, D.G. and GORDON, M.P. (1967) Ultraviolet photoinactivation studies on hybrid viruses obtained by the cross-reconstitution of the protein and RNA components of U(1) and U(2) strains of TMV. *Photochem. Photobiol.* **6**, 413-421.

WANG, J., MAUSER, A., CHAO, S.F., REMINGTON, K., TRECKMANN, R., KAISER, K., PIFAT, D. and HOTTA, J. (2004) Virus inactivation and protein recovery in a novel ultraviolet-C reactor. *Vox Sang*. **86**, 230-238.

WHO Technical Report, (2004) Guidelines on viral inactivation and removal procedures intended to assure the viral safety of human blood plasma products, **924**, 150-224.

WOLF, A., MASON, J., FITZPATRICK, W.J., SCHWARTZ, S.O. and LEVINSON, S.O., (1947). Ultraviolet irradiation of human plasma to control homologous serum jaundice. *J. Am. Med. Assoc.* **135**, 476-477.

